Acta Mech 234, 4629–4647 (2023)
https://doi.org/10.1007/s00707-023-03626-y

ORIGINAL PAPER

**Mingliang Jiang · Xinwei Du · Arun Srinivasa · Jimin Xu · Zhujiang Wang**

# Reformulation of the virtual fields method using the variation of elastic energy for parameter identification of QR decomposition-based hyperelastic models

Received: 21 March 2023 / Revised: 29 May 2023 / Accepted: 6 June 2023 / Published online: 25 June 2023


**Abstract** **QR** decomposition-based constitutive relations for hyperelastic materials have attracted great attention from the community of solid mechanics, as hyperelastic models in terms of the distortion tensor $\widetilde{\boldsymbol{F}}$ have obvious physical meanings. However, there are few works systematically discussing the material parameter identification for **QR** decomposition-based hyperelastic models. In this work, we reformulate the virtual fields method by considering the internal virtual work as the variation of elastic energy caused by virtual displacements. This approach (together with the **QR** decompositions) is more concise and easier to be implemented when compared with the conventional approach, which requires specific stresses, such as Cauchy stress, first or second Piola–Kirchhoff stress, and conjugate virtual strains to calculate the internal virtual work. To validate the reformulated virtual fields method, we derive the Mooney–Rivlin model under the **QR** framework, and then identify its material parameters for incompressible silicone specimens under biaxial tensile tests. The results indicate that the proposed virtual fields method works very well for **QR** decomposition-based models.

## 1 Introduction

The community of solid mechanics widely adopts the concept of the polar decomposition of the deformation gradient $\mathbf{F} = \mathbf{RU} = \mathbf{VR}$, where $\mathbf{R}$ represents the rotation; the symmetric tensors $\mathbf{U}$ and $\mathbf{V}$ describe the stretch. The **QR** decomposition (also called upper triangular decomposition), an alternative to the polar decomposition, was first introduced by McLellan [1,2], where he separated the deformation gradient into an orthogonal matrix

M. Jiang · J. Xu
School of Mechanical Engineering, Hefei University of Technology, Hefei 230009, Anhui, China
E-mail: mingliang.jiang@hfut.edu.cn

J. Xu
E-mail: xujimin2017@hfut.edu.cn

X. Du · Z. Wang (✉)
Department of Mechanical Engineering (Robotics), Guangdong Technion - Israel Institute of Technology, Shantou 515063, Guangdong, China
E-mail: xinwei.du@gtiit.edu.cn

Z. Wang
E-mail: zhujiang.wang@gtiit.edu.cn

A. Srinivasa
Department of Mechanical Engineering, Texas A&M University, College Station, TX 77843, USA

A. Srinivasa
E-mail: asrinivasa@tamu.edu

and an upper triangular matrix with positive diagonal elements. Over the last decade, Srinivasa et al. [3–6] visited this decomposition anew and proposed mechanical theories based on **QR** decomposition, in which the deformation gradient is decomposed as $\mathbf{F} = \mathbf{Q}\widetilde{\boldsymbol{F}}$, where $\mathbf{Q}$ is a rotation matrix and the upper triangular tensor $\widetilde{\boldsymbol{F}}$ is referred to as the distortion tensor. Note that this distortion tensor was also called “Laplace stretch" by Freed et al. [7,8].

Compared with the polar decomposition, the **QR** decomposition has the following advantages: (1) it exploits natural directions either in the structure of anisotropic materials or in the choice of laboratory axes instead of the fixed Cartesian coordinate system; (2) the six components of $\widetilde{\boldsymbol{F}}$ have direct physical meanings in terms of pure stretch or simple shear deformations; (3) the upper triangular matrices are closed under operations of addition and multiplication; (4) the components of the Cauchy stress are related in a simpler manner to the derivatives of strain energy density function with respect to the components of $\widetilde{\boldsymbol{F}}$ when compared with those based on the invariants of the strain tensor. These advantages make it appealing to use as a measure of strain. Freed and Srinivasa [5] introduced the logarithm of distortion tensor as a new strain measure and contrasted it with Hencky strain (the logarithm of stretch) for three sets of experiments including shear-free deformation, simple shear, and pure shear. The result for simple shear showed that the new strain measure depended linearly on the shear amount, which was distinct from the non-monotonic behavior of the logarithm of stretch. Gao and Li [9] proved that there existed in total six possibilities of decomposing the distortion tensor into a product of matrices for one triaxial stretch and two simple shear deformations and total twenty-four cases for decomposition of $\widetilde{\boldsymbol{F}}$ into a product of matrices for one triaxial stretch and three simple shear deformations.

Constitutive modeling of hyperelastic materials based on the **QR** decomposition of the deformation gradient (we call this **QR** framework in the rest of this paper for simplicity) attracted researchers' attention in recent years. Li and Gao [10] derived constitutive equations for hyperelastic materials including unconstrained and incompressible isotropic materials, incompressible transversely isotropic composite materials, and incompressible orthotropic composite materials using strain energy density functions based on the **QR** decomposition. They demonstrated that relating the Cauchy stress directly to derivatives of the strain energy density functions with respect to the components of distortion tensor led to simpler and more explicit expressions. Salamatova et al. [11] presented a method to model the deformation of hyperelastic materials under finite strains with the new strain measure based on **QR** decomposition. Annin and Bagrov [12] introduced this strain measure into numerical simulations for an arbitrary three-dimensional model. Freed and Zamani [13] derived components for a metric tensor, its dual, and their rates which describe any state of deformation in a convected coordinate system and are expressed in terms of physical attributes arising from **QR** decomposition. Continuing on this work, they derived a model for porcine coronary sinus tissue, a soft biological tubular structure [14]. Clayton and Freed [15] developed a novel theoretical framework under the context of **QR** decomposition which encompasses viscoelasticity and damage. This is the first time that **QR** kinematics have been applied to these phenomena. They further constructed a continuum model for lung parenchyma capable of describing its thermomechanical response over a large range of loading rates and stress states [16].

Inspired by Li and Gao's work on neo-Hookean model under the **QR** framework [10], the Mooney–Rivlin model [17] is derived and expressed in terms of the distortion tensor $\widetilde{\boldsymbol{F}}$. While researchers have started exploring the **QR** decomposition-based hyperelastic models, to the best of the authors' knowledge, there are only a few pieces of work discussing the method to extract parameters of the **QR** decomposition-based hyperelastic models. Since uniaxial testing only is not enough to fully investigate the mechanical properties of hyperelastic materials [18], we focus on extracting the mechanical properties of hyperelastic materials under biaxial tensile tests with full-field deformation data using the virtual fields method (VFM), which has proved to be an accurate and efficient inverse method in parameter identification of invariant-based hyperelastic models [19–22]. However, implementing the procedure of the conventional VFM directly into the **QR** decomposition-based hyperelastic models needs first to calculate stresses and conjugate virtual strains, which requires extra mathematical derivations and calculations. Therefore, we reformulate the VFM based on the variation of elastic energy to extract parameters of hyperelastic models under the **QR** framework.

The rest of the paper is organized as follows. Section 2 briefly reviews **QR** decomposition-based hyperelastic models, and proposes the reformulation of VFM based on the variation of elastic energy. Section 3 describes the experimental setup, materials, testing methods, construction of virtual fields, and procedure of parameter identification. In Sect. 4, the results of parameter identification of **QR** decomposition-based hyperelastic models are presented; Cauchy stress is reconstructed under both the frameworks of polar decomposition and **QR** decomposition. Section 5 summarizes the study.

## 2 Theory

### 2.1 Hyperelastic models under **QR** framework

Under the **QR** framework, the deformation gradient $\mathbf{F}$ can be rewritten as $\mathbf{F} = \mathbf{f_i} \otimes \mathbf{e_i}$ [3,9], where $\mathbf{e_i}$ (i = 1, 2, 3) are three base vectors of a Cartesian coordinate system, and can be uniquely decomposed as $\mathbf{F} = \mathbf{Q}\widetilde{\boldsymbol{F}}$, where $\mathbf{Q} = \mathbf{e_i'} \otimes \mathbf{e_i}$ is a rotation matrix,

$$\mathbf{e_1}' = \frac{\mathbf{f_1}}{|\mathbf{f_1}|}, \mathbf{e_2}' = \frac{\mathbf{f_2} - (\mathbf{f_2} \cdot \mathbf{e_1}')\mathbf{e_1}'}{|\mathbf{f_2} - (\mathbf{f_2} \cdot \mathbf{e_1}')\mathbf{e_1}'|}, \mathbf{e_3}' = \mathbf{e_1}' \times \mathbf{e_2}'. \tag{1}$$

and $\widetilde{\boldsymbol{F}}$ is an upper triangular matrix that represents distortion where

$$[\widetilde{F}_{ij}] = \begin{bmatrix} \widetilde{F}_{11} & \widetilde{F}_{12} & \widetilde{F}_{13} \\ 0 & \widetilde{F}_{22} & \widetilde{F}_{23} \\ 0 & 0 & \widetilde{F}_{33} \end{bmatrix} \tag{2}$$

with

$$\begin{aligned} &\widetilde{F}_{11} = \sqrt{C_{11}} \\ &\widetilde{F}_{12} = \frac{C_{12}}{\widetilde{F}_{11}}, \qquad \widetilde{F}_{22} = \sqrt{C_{22} - \widetilde{F}_{12}^2} \\ &\widetilde{F}_{13} = \frac{C_{13}}{\widetilde{F}_{11}}, \qquad \widetilde{F}_{23} = \frac{C_{23} - \widetilde{F}_{12}\widetilde{F}_{13}}{\widetilde{F}_{22}}, \qquad \widetilde{F}_{33} = \sqrt{C_{33} - \widetilde{F}_{23}^2 - \widetilde{F}_{13}^2}. \end{aligned} \tag{3}$$

where $C_{ij}$ are the components of the right Cauchy–Green deformation tensor $\mathbf{C}$ ($\mathbf{C} = \mathbf{F}^T\mathbf{F} = \widetilde{\mathbf{F}}^T\widetilde{\mathbf{F}}$). Consequently, the first and second invariants of right Cauchy–Green strain tensor $\mathbf{C}$ can be obtained as

$$\begin{aligned} I_1 &= tr(\mathbf{C}) = \widetilde{F}_{11}^2 + \widetilde{F}_{12}^2 + \widetilde{F}_{22}^2 + \widetilde{F}_{13}^2 + \widetilde{F}_{23}^2 + \widetilde{F}_{33}^2 \\ I_2 &= \frac{1}{2}((tr(\mathbf{C})^2 - tr(\mathbf{C}^2)) \\ &= \widetilde{F}_{11}^2\widetilde{F}_{22}^2 + \widetilde{F}_{11}^2\widetilde{F}_{23}^2 + \widetilde{F}_{11}^2\widetilde{F}_{33}^2 + \widetilde{F}_{12}^2\widetilde{F}_{23}^2 + \widetilde{F}_{12}^2\widetilde{F}_{33}^2 \\ &\quad + \widetilde{F}_{22}^2\widetilde{F}_{13}^2 + \widetilde{F}_{22}^2\widetilde{F}_{33}^2 - 2\widetilde{F}_{12}\widetilde{F}_{13}\widetilde{F}_{22}\widetilde{F}_{23} \end{aligned} \tag{4}$$

With $I_1$ and $I_2$ expressed in terms of $\widetilde{F}_{ij}$, invariant-based constitutive models for incompressible hyperelastic materials can be formulated under the **QR** framework, $W = W(\mathbf{C}) = \bar{W}(\widetilde{\boldsymbol{F}})$. By substituting the first invariant part of Eq. (4) into neo-Hookean model, Li and Gao [10] obtained the strain energy density function as

$$\bar{W}_{NH}(\widetilde{\boldsymbol{F}}) = C_{10}(\widetilde{F}_{11}^2 + \widetilde{F}_{12}^2 + \widetilde{F}_{22}^2 + \widetilde{F}_{13}^2 + \widetilde{F}_{23}^2 + \widetilde{F}_{33}^2 - 3) \tag{5}$$

Inspired by their work on neo-Hookean model, we derive the Mooney–Rivlin model under **QR** framework which is expressed as

$$\begin{aligned} \bar{W}_{MR}(\widetilde{\boldsymbol{F}}) &= C_{10}(\widetilde{F}_{11}^2 + \widetilde{F}_{12}^2 + \widetilde{F}_{22}^2 + \widetilde{F}_{13}^2 + \widetilde{F}_{23}^2 + \widetilde{F}_{33}^2 - 3) \\ &\quad + C_{01}(\widetilde{F}_{11}^2\widetilde{F}_{22}^2 + \widetilde{F}_{11}^2\widetilde{F}_{23}^2 + \widetilde{F}_{11}^2\widetilde{F}_{33}^2 + \widetilde{F}_{12}^2\widetilde{F}_{23}^2 + \widetilde{F}_{12}^2\widetilde{F}_{33}^2 \\ &\quad + \widetilde{F}_{22}^2\widetilde{F}_{13}^2 + \widetilde{F}_{22}^2\widetilde{F}_{33}^2 - 2\widetilde{F}_{12}\widetilde{F}_{13}\widetilde{F}_{22}\widetilde{F}_{23} - 3) \end{aligned} \tag{6}$$

The components of the distortion tensor $\widetilde{\boldsymbol{F}}$ in **QR** decomposition-based neo-Hookean model and Mooney–Rivlin model have direct physical meaning in terms of simple shear deformations and stretches [3]. Compared to conventional invariant-based hyperelastic models built directly upon $\mathbf{F}$, the models based on the **QR** decomposition have significant advantages in addressing noisy data [23]. Additionally, the **QR** decomposition-based hyperelastic models can be easily extended to orthotropic materials [3], eliminating the challenges associated with the substantial covariance between different modes of deformation, which the conventional invariant-based approach cannot avoid [24].

In this paper, biaxial tests were conducted on very thin silicone membranes; thus, we assume that the out-of-plane shearing is negligible and the material is incompressible. Therefore, the invariants in Eq. (4) can be simplified as

$$\begin{aligned} I_1 &= tr(\mathbf{C}) = \widetilde{F}_{11}^2 + \widetilde{F}_{12}^2 + \widetilde{F}_{22}^2 + \widetilde{F}_{33}^2 \\ I_2 &= \frac{1}{2}((tr(\mathbf{C})^2 - tr(\mathbf{C}^2)) = \widetilde{F}_{11}^2\widetilde{F}_{22}^2 + \widetilde{F}_{11}^2\widetilde{F}_{33}^2 + \widetilde{F}_{12}^2\widetilde{F}_{33}^2 + \widetilde{F}_{22}^2\widetilde{F}_{33}^2 \end{aligned} \tag{7}$$

with $\widetilde{F}_{33} = \frac{1}{\widetilde{F}_{11}\widetilde{F}_{22}}$. The **QR** decomposition-based hyperelastic models in Eqs. (5) and (6) can be simplified as

$$\bar{W}_{NH}(\widetilde{\boldsymbol{F}}) = C_{10}(\widetilde{F}_{11}^2 + \widetilde{F}_{12}^2 + \widetilde{F}_{22}^2 + \widetilde{F}_{33}^2 - 3) \tag{8}$$

and

$$\begin{aligned} \bar{W}_{MR}(\widetilde{\boldsymbol{F}}) = {} & C_{10}(\widetilde{F}_{11}^2 + \widetilde{F}_{12}^2 + \widetilde{F}_{22}^2 + \widetilde{F}_{33}^2 - 3) \\ & + C_{01}(\widetilde{F}_{11}^2\widetilde{F}_{22}^2 + \widetilde{F}_{11}^2\widetilde{F}_{33}^2 + \widetilde{F}_{12}^2\widetilde{F}_{33}^2 + \widetilde{F}_{22}^2\widetilde{F}_{33}^2 - 3) \end{aligned} \tag{9}$$

## 2.2 Reformulation of the VFM using the variation of elastic energy

Assuming that loading processes are quasi-static and the body force is negligible, a conventional VFM [20] can be expressed as

$$-\int_{\Omega_0} \mathbf{P} : Grad(\mathbf{U}^*)dV + \int_{\Gamma_0} \mathbf{T} \cdot \mathbf{U}^* dS = 0 \tag{10}$$

where $\mathbf{P}$ is the first Piola–Kirchhoff stress, $\mathbf{T}$ represents the traction vector prescribed at the boundary $\Gamma_0$ of the specimen with the surface area $S$, $\mathbf{U}^*$ is the virtual displacement vector defined in the reference configuration. The first term of Eq. (10) is the virtual work done by the internal force, and thus can be considered as internal virtual work (IVW); the second term of this equation is the virtual work done by the external force and can be taken as external virtual work (EVW). According to the conventional parameter identification procedure using VFM [21], for incompressible materials, the first Piola–Kirchhoff stress tensor $\mathbf{P}$ can be obtained as

$$\mathbf{P} = -p\mathbf{F}^{-T} + \frac{\partial W}{\partial \mathbf{F}} \tag{11}$$

where $p$ is an arbitrary hydrostatic pressure that ensures the material incompressibility, $\mathbf{F}$ is the deformation gradient tensor, and $W$ is the strain energy density function. The IVW expressed in Eq. (10) can also be expressed in terms of Cauchy stress or the second Piola–Kirchhoff stress together with their conjugate virtual strains [25].

Note that the conventional VFM must select one of the three types of stresses discussed earlier and their conjugate virtual strains [25]. When dealing with principal stretch-based hyperelastic models, such as the Ogden model, which can only yield principal stresses directly, it is necessary to perform stress transformation [21], which can lead to extra mathematical derivations and calculations. Considering that the VFM is originally derived based on the principle of virtual work, the IVW is essentially the variation of the elastic energy caused by virtual displacements. Therefore, we reformulate it in the following form

$$IVW = \int_{V_0} \delta W \left(\mathbf{x}(\mathbf{X}), \mathbf{U}^*\right) \, dV \tag{12}$$

where $W$ is the strain energy density function of the hyperelastic material; $\delta W(\mathbf{x}(\mathbf{X}), \mathbf{U}^*)$ is the variation of $W$ caused by the virtual displacement $\mathbf{U}^*$. The details of calculating IVW for invariant, principal stretch, and **QR** decomposition-based hyperelastic models using the reformulated VFM are discussed in the following subsections.

### 2.2.1 Derivation of IVW for invariant-based hyperelastic models

Invariant-based hyperelastic models, such as neo-Hookean and Mooney–Rivlin models, are the most popular type of hyperelastic constitutive relations. Therefore, in this section, we derive the IVW for conventional incompressible invariant-based hyperelastic models, such as Mooney–Rivlin model,[1] to demonstrate the convenience of the reformulated VFM based on the variation of elastic energy. According to Eq. (12), the IVW for an incompressible Mooney–Rivlin model can be expressed as

$$\begin{aligned} IVW_{MR} &= \int_{V_0} \delta W(I_1, I_2)\, dV = \int_{V_0} \frac{\partial W(I_1, I_2)}{\partial \mathbf{F}} : \delta \mathbf{F}\, dV \\ &= \int_{V_0} \left( C_{10} \frac{\partial I_1}{\partial \mathbf{F}} + C_{01} \frac{\partial I_2}{\partial \mathbf{F}} \right) : \delta \mathbf{F}\, dV \end{aligned} \tag{13}$$

where $\delta \mathbf{F} = \frac{\partial \mathbf{U}^*}{\partial \mathbf{X}}$, and $\mathbf{U}^*$ is the virtual displacement. Due to the incompressibility and the membrane assumption for specimens under tensile tests, the first and second invariants of the right Cauchy–Green deformation tensor can be written in the form of the components of deformation gradient $\mathbf{F}$

$$\begin{aligned} I_1 &= tr(\mathbf{C}) = F_{11}^2 + F_{21}^2 + F_{12}^2 + F_{22}^2 + \frac{1}{D^2} \\ I_2 &= \frac{1}{2}(tr(\mathbf{C})^2 - tr(\mathbf{C}^2)) = D^2 + \frac{F_{11}^2 + F_{21}^2 + F_{12}^2 + F_{22}^2}{D^2} \end{aligned} \tag{14}$$

with $D = \frac{1}{F_{33}} = F_{11}F_{22} - F_{12}F_{21}$. Note that we can also calculate the IVW in Eq. 13 directly based on $\delta W(I_1, I_2) = \frac{\partial W(I_1, I_2)}{\partial I_1}\delta I_1 + \frac{\partial W(I_1, I_2)}{\partial I_2}\delta I_2 = C_{10}\delta I_1 + C_{01}\delta I_2$, with $\delta I_1$ and $\delta I_2$ as

$$\begin{aligned} \delta I_1 &= 2\left(F_{11} - \frac{F_{22}}{D^3}\right)\delta F_{11} + 2\left(F_{12} + \frac{F_{21}}{D^3}\right)\delta F_{12} \\ &\quad + 2\left(F_{21} + \frac{F_{12}}{D^3}\right)\delta F_{21} + 2\left(F_{22} - \frac{F_{11}}{D^3}\right)\delta F_{22} \\ \delta I_2 &= 2\left(F_{22}D + \frac{F_{11}}{D^2} - \frac{F_{22}(F_{11}^2 + F_{21}^2 + F_{12}^2 + F_{22}^2)}{D^3}\right)\delta F_{11} \\ &\quad + 2\left(-F_{21}D + \frac{F_{12}}{D^2} + \frac{F_{21}(F_{11}^2 + F_{21}^2 + F_{12}^2 + F_{22}^2)}{D^3}\right)\delta F_{12} \\ &\quad + 2\left(-F_{12}D + \frac{F_{21}}{D^2} + \frac{F_{12}(F_{11}^2 + F_{21}^2 + F_{12}^2 + F_{22}^2)}{D^3}\right)\delta F_{21} \\ &\quad + 2\left(F_{11}D + \frac{F_{22}}{D^2} - \frac{F_{11}(F_{11}^2 + F_{21}^2 + F_{12}^2 + F_{22}^2)}{D^3}\right)\delta F_{11} \end{aligned} \tag{15}$$

The above derivation of IVW can be easily extended to any incompressible hyperelastic models expressed in terms of the first and/or the second invariant. The formulation of IVW using Eq. 13 is equivalent to Promma and Grediac's approach [20] (see "Appendix A" for the derivation procedure). Therefore, for invariant-based hyperelastic models, the variation of elastic energy-based virtual fields method (VEE-VFM) is equivalent to the conventional VFM in the aspect of computational complexity to calculate the IVW. However, a conjugate pair of stresses and virtual strains are required to be selected explicitly for conventional VFM, while this is automatically guaranteed in VEE-VFM; thus, VEE-VFM for invariant-based hyperelastic models should be more friendly to novice researchers and engineers. A flowchart about the comparison between the conventional VFM and VEE-VFM is shown in Fig. 1. Note that there are many approaches to calculating the IVW using the conventional VFM, the selected one in Fig. 1b is based on the first Piola–Kirchhoff stress, and is one of the most popular approaches adopted by researchers [20,21,26,27].

[1] The derivation for the IVW of neo-Hookean model is similar (let $C_{01} = 0$).

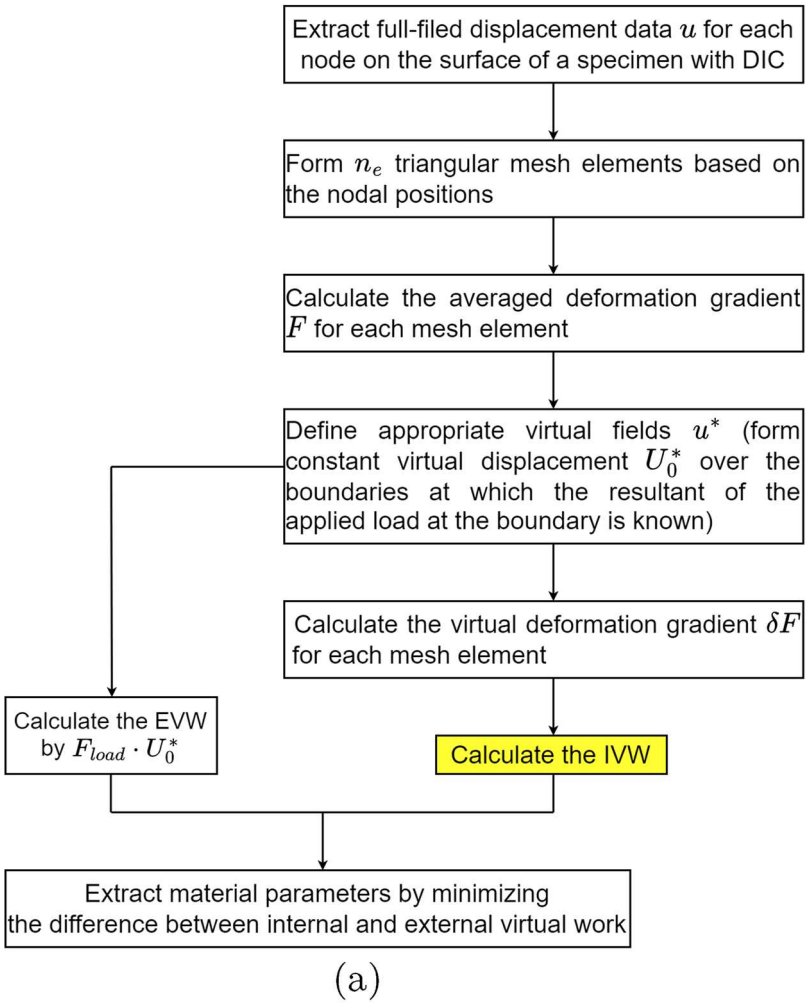


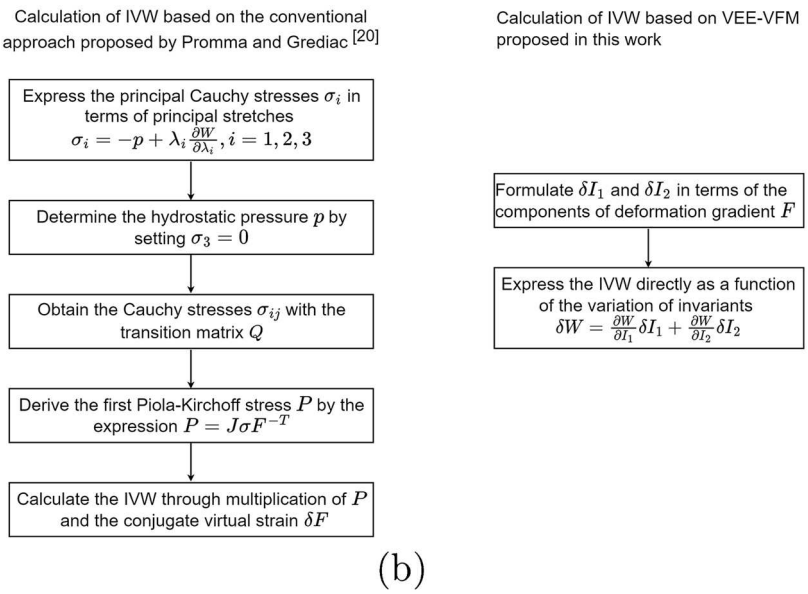


**Fig. 1** **a** Flowchart for the procedure of parameter identification based on the conventional VFM and the VEE-VFM proposed in this work. The step colored in yellow denotes the calculation of IVW; **b** the comparison between the conventional approach proposed by Promma and Grediac [20] and the VEE-VFM in calculating the IVW

### 2.2.2 Derivation of IVW for principal stretch-based hyperelastic models

Principal stretch-based hyperelastic models are another popular type of hyperelastic constitutive relations. For instance, Ogden model is widely adopted in the modeling of hyperelastic materials. Following conventional procedures to calculate the IVW [21], the principal first Piola–Kirchhoff stress $\mathbf{P}_a$ is determined first; the first Piola–Kirchhoff stress $\mathbf{P}$ can then be obtained based on the principal stress $\mathbf{P}_a$ through stress transformation; the conjugate virtual strain $\delta\mathbf{F}$ is calculated in the next step; finally, the IVW is equal to the integration of the product of the first Piola–Kirchhoff stress and its conjugate virtual strain $\int \mathbf{P} : \delta\mathbf{F}\, dV_0$.

As an alternative approach, we can calculate the IVW based on the variation of elastic energy (see Eq. (12)). For example, the IVW for principal stretch-based hyperelastic models of compressible materials can be expressed as

$$\begin{aligned} IVW &= \int_{V_0} \delta W(\lambda_1, \lambda_2, \lambda_3)\, dV = \int_{V_0} \frac{\partial W}{\partial \lambda_a} \delta\lambda_a\, dV \\ &= \int_{V_0} \frac{\partial W}{\partial \lambda_a} \frac{1}{2\lambda_a} [\mathbf{N}_a \otimes \mathbf{N}_a]_{ij} (\delta F_{ki} F_{kj} + F_{ki} \delta F_{kj})\, dV \end{aligned} \tag{16}$$

where $\frac{\partial W}{\partial \lambda_a}$ is essentially the principal first Piola–Kirchhoff stress, which can be represented by $P_a = \frac{\partial W}{\partial \lambda_a}$; $\lambda_a^2$ are the eigenvalues (squares of principal stretches) and $\mathbf{N}_a$ is the corresponding eigenvector (principal referential directions) of $\mathbf{C}$. For incompressible materials under tensile tests with plane-stress assumption, we can simply let $\lambda_3 = 1/\lambda_1\lambda_2$ and substitute it into Eq. (16) to calculate the IVW, where $\lambda_3$ is the principal stretch in the out-of-plane direction. It is obvious that the VEE-VFM for the principal stretch-based hyperelastic models has the following advantages: (a) it can automatically ensure that the stress ($\mathbf{P}_a$) and virtual strain ($\delta\lambda_a$) are conjugate; (b) there is no need to transform the principal first Piola–Kirchhoff stress $\mathbf{P}_a$ to the first Piola–Kirchhoff stress $\mathbf{P}$ used in conventional VFM. These advantages also apply to **QR** decomposition-based hyperelastic models, which will be discussed in the next subsection.

### 2.2.3 Derivation of IVW for *QR* decomposition-based hyperelastic models

The main objective of this work is to develop the VFM to extract material parameters of **QR** decomposition-based hyperelastic models. Following the conventional VFM and the current theory on **QR** decomposition-based hyperelastic models, we need to calculate the rotated Cauchy stress, which needs to be transformed to the first Piola–Kirchhoff stress to calculate the IVW, and this transformation will include complicated mathematical derivations. However, we can calculate the IVW for **QR** decomposition-based hyperelastic models in a much more concise way using VEE-VFM. Taking the **QR** decomposition-based Mooney–Rivlin model as an example, the IVW is expressed as

$$\begin{aligned} IVW &= \int_{V_0} \delta\bar{W}(\widetilde{\boldsymbol{F}})_{MR}\, dV = \int_{V_0} \frac{\partial \bar{W}}{\partial \widetilde{\boldsymbol{F}}} : \delta\widetilde{\boldsymbol{F}}\, dV \\ &= \int_{V_0} \left( C_{10} \frac{\partial I_1(\widetilde{\boldsymbol{F}})}{\partial \widetilde{\boldsymbol{F}}} + C_{01} \frac{\partial I_2(\widetilde{\boldsymbol{F}})}{\partial \widetilde{\boldsymbol{F}}} \right) : \delta\widetilde{\boldsymbol{F}}\, dV \end{aligned} \tag{17}$$

where $\frac{\partial \bar{W}}{\partial \widetilde{\boldsymbol{F}}} = C_{10} \frac{\partial I_1(\widetilde{\boldsymbol{F}})}{\partial \widetilde{\boldsymbol{F}}} + C_{01} \frac{\partial I_2(\widetilde{\boldsymbol{F}})}{\partial \widetilde{\boldsymbol{F}}}$ can be considered as a rotated first Piola–Kirchhoff stress $\widetilde{\boldsymbol{P}}$, and the details about $\delta\widetilde{\boldsymbol{F}}$ is discussed in the following part.

Assuming that the specimen under tensile tests is an incompressible membrane, we can obtain

$$\begin{aligned} \widetilde{F}_{11} &= \sqrt{F_{11}^2 + F_{21}^2} \\ \widetilde{F}_{12} &= \frac{F_{11}F_{12} + F_{21}F_{22}}{\sqrt{F_{11}^2 + F_{21}^2}} \\ \widetilde{F}_{22} &= \sqrt{F_{12}^2 + F_{22}^2 - \frac{(F_{11}F_{12} + F_{21}F_{22})^2}{F_{11}^2 + F_{21}^2}} \end{aligned}$$

$$\widetilde{F}_{33} = \sqrt{\frac{1}{(F_{11}F_{22} - F_{12}F_{21})^2}} = F_{33} \tag{18}$$

Therefore, we have

$$\begin{aligned}
\delta\widetilde{F}_{11} &= \frac{\partial\widetilde{F}_{11}}{\partial F_{11}}\delta F_{11} + \frac{\partial\widetilde{F}_{11}}{\partial F_{21}}\delta F_{21} \\
\delta\widetilde{F}_{12} &= \frac{\partial\widetilde{F}_{12}}{\partial F_{11}}\delta F_{11} + \frac{\partial\widetilde{F}_{12}}{\partial F_{12}}\delta F_{12} + \frac{\partial\widetilde{F}_{12}}{\partial F_{21}}\delta F_{21} + \frac{\partial\widetilde{F}_{12}}{\partial F_{22}}\delta F_{22} \\
\delta\widetilde{F}_{22} &= \frac{\partial\widetilde{F}_{22}}{\partial F_{11}}\delta F_{11} + \frac{\partial\widetilde{F}_{22}}{\partial F_{12}}\delta F_{12} + \frac{\partial\widetilde{F}_{22}}{\partial F_{21}}\delta F_{21} + \frac{\partial\widetilde{F}_{22}}{\partial F_{22}}\delta F_{22} \\
\delta\widetilde{F}_{33} &= \frac{\partial\widetilde{F}_{33}}{\partial F_{11}}\delta F_{11} + \frac{\partial\widetilde{F}_{33}}{\partial F_{12}}\delta F_{12} + \frac{\partial\widetilde{F}_{33}}{\partial F_{21}}\delta F_{21} + \frac{\partial\widetilde{F}_{33}}{\partial F_{22}}\delta F_{22}
\end{aligned} \tag{19}$$

The detailed expression of the above four terms can be found in "Appendix B". With the elastic energy $\bar{W}(\widetilde{\boldsymbol{F}})$ expressed in terms of $\widetilde{\boldsymbol{F}}$, the derivation of IVW can be easily extended to any incompressible **QR** decomposition-based hyperelastic models. Note that given $I_1(\widetilde{\boldsymbol{F}})$ and $I_2(\widetilde{\boldsymbol{F}})$ in Eq. (7), we can also calculate the IVW in Eq. 17 based on

$$\delta\bar{W}_{MR}(\widetilde{\boldsymbol{F}}) = \frac{\partial\bar{W}}{\partial I_1}\delta I_1(\widetilde{\boldsymbol{F}}) + \frac{\partial\bar{W}}{\partial I_2}\delta I_2(\widetilde{\boldsymbol{F}}) = C_{10}\delta I_1(\widetilde{\boldsymbol{F}}) + C_{01}\delta I_2(\widetilde{\boldsymbol{F}}) \tag{20}$$

with

$$\begin{aligned}
\delta I_1(\widetilde{\boldsymbol{F}}) &= 2(\widetilde{F}_{11}\delta\widetilde{F}_{11} + \widetilde{F}_{12}\delta\widetilde{F}_{12} + \widetilde{F}_{22}\delta\widetilde{F}_{22} + \widetilde{F}_{33}\delta\widetilde{F}_{33}) \\
\delta I_2(\widetilde{\boldsymbol{F}}) &= 2(\widetilde{F}_{11}\widetilde{F}_{22}^2\delta\widetilde{F}_{11} + \widetilde{F}_{22}\widetilde{F}_{11}^2\delta\widetilde{F}_{22} + \widetilde{F}_{11}\widetilde{F}_{33}^2\delta\widetilde{F}_{11} + \widetilde{F}_{33}\widetilde{F}_{11}^2\delta\widetilde{F}_{33} \\
&\quad + \widetilde{F}_{12}\widetilde{F}_{33}^2\delta\widetilde{F}_{12} + \widetilde{F}_{33}\widetilde{F}_{12}^2\delta\widetilde{F}_{33} + \widetilde{F}_{22}\widetilde{F}_{33}^2\delta\widetilde{F}_{22} + \widetilde{F}_{33}\widetilde{F}_{22}^2\delta\widetilde{F}_{33})
\end{aligned} \tag{21}$$

Up to now, we have derived the IVW for invariant, principal stretch, and **QR** decomposition-based hyperelastic models using the variation of elastic energy. It is worth noting that the method to calculate the IVW in the VEE-VFM is more fundamental when compared with conventional VFM, as the IVW in the VEE-VFM is directly considered as the variation of elastic energy caused by virtual displacements. Therefore, calculating IVW in the VEE-VFM does not require any particular attention to the conjugate relation between stresses and virtual strains because it is automatically guaranteed. Additionally, calculating the IVW for principal stretch and **QR** decomposition-based hyperelastic models using VEE-VFM does not require any stress transformation, and thus it is more concise and researchers are less likely to make mistakes.

## 3 Experiments and application of VEE-VFM

### 3.1 Experimental setup and specimen preparation

Three cruciform specimens were laser cut from a silicone sheet with a thickness of 0.508 mm (Specialty Manufacturing Incorporation, Saginaw, MI, USA). The arm width of the specimen was 12.7 mm. The specimen was mounted on a biaxial testing platform with an initial grip distance of 50.8 mm. As shown in Fig. 2, the testing system is composed of four linear actuators which can drive the specimen from four directions simultaneously. Forces were measured by load cells with capacities of 10 lbfs, and displacements were measured by linear variable differential transformers (LVDTs). A digital PID controller was implemented to provide closed-loop feedback control of the system. Each specimen was first subjected to ten preconditioning cycles with a global strain of 1.7 along both axes at a strain rate of 0.01 $s^{-1}$ and was then allowed to recover for 15 min. Note that the global strain was calculated as the ratio between the grip separation distance and the initial grip distance. Then, four strain-controlled biaxial tests were conducted with a maximum value of 1.5, with axial strain ratios of $\lambda_{11}$:$\lambda_{22}$ = 1:1, 1:0.5, 0.5:1, 1:1. Note that '1' refers to the maximum strain of 1.5, and '0.5' refers to half of the maximum strain, which is 1.25. The recovery time was set as 15 min between each test. Images were captured by an area scan camera with a resolution of 2048 × 2048 $pixels^2$ at every two seconds and synchronized with

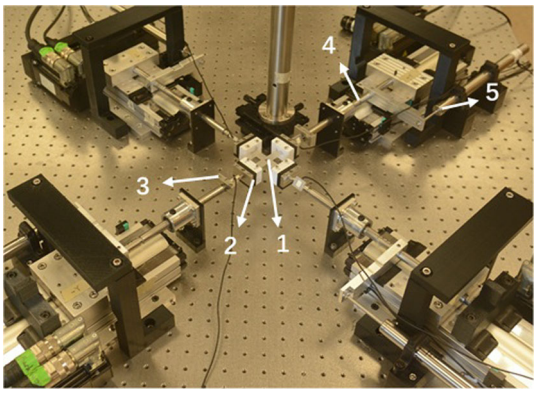


**Fig. 2** Biaxial testing platform. (1) Silicone elastomer, (2) clamp, (3) load cell, (4) linear actuator, (5) LVDT

**Table 1** DIC settings used in image analysis

| Parameters | Settings |
|---|---|
| Subset radius | 21 pixels |
| Step size | 7 pixels |
| Strain window radius | 8 pixels |
| Subset shape function | Affine |
| Interpolation | Biquintic B-spline |
| Matching criterion | Normalized cross-correlation(NCC) |
| Image scale | 0.0395 mm/pixel |

the data acquisition device. Twenty-six images including the initial undeformed stage were acquired for each biaxial test. Details about the testing system and protocols can be found in this paper [28]. The last 1:1 test run (equi-biaxial test) was selected for study in this paper. A Matlab-based DIC software, Ncorr [29], was used for strain calculation with a subset radius of 21 pixels and a step size of 7 pixels chosen for this study. The DIC settings used for image analysis are listed in Table 1.

### 3.2 Construction of virtual fields

Virtual fields were constructed for a cruciform specimen under a biaxial tensile test across a selected Region of Interest (ROI) as follows [26,30].

$$U^{*(a)} = \begin{cases} U_x^* = \frac{X-X_c}{W} \\ U_y^* = 0 \end{cases} \tag{22a}$$

$$U^{*(b)} = \begin{cases} U_x^* = 0 \\ U_y^* = \frac{Y-Y_c}{H} \end{cases} \tag{22b}$$

$$U^{*(c)} = \begin{cases} U_x^* = \frac{Y-Y_c}{|Y-Y_c|} \sin\left(\frac{X-X_c}{W}\pi\right) \sin\left(\frac{Y-Y_c}{H}\pi\right) \\ U_y^* = \frac{X-X_c}{|X-X_c|} \sin\left(\frac{X-X_c}{W}\pi\right) \sin\left(\frac{Y-Y_c}{H}\pi\right) \end{cases} \tag{22c}$$

where $H$ and $W$ are halves of the height and the width of the selected cruciform ROI where the virtual fields are defined, respectively. $X$ and $Y$ represent the coordinates in the global frame regarding the initial configuration, $(X_c, Y_c)$ is the coordinate of the center of the ROI. The first two virtual fields allow us to write the EVW for the applied load along the x- and y-directions, respectively. For example, the first virtual field creates uniform virtual displacement at both the left and right boundaries of the selected ROI of the cruciform specimen, which is 1 mm. Therefore, the EVW can be calculated as the summation of the multiplication between the applied force $F_x$ and virtual displacement at both left and right boundaries in the x-direction, which is $2 * F_x * 1$ mm. Similarly, the EVW for the second virtual field can be calculated as the summation of

the multiplication between the applied force $F_y$ and virtual displacement at both top and bottom boundaries in the y-direction, which is $2 * F_y * 1$ mm. The third virtual field activates all the components of the stress tensor in calculation of the IVW, and the corresponding EVW is zero since the virtual displacements at all the boundaries are zero. Similar virtual fields can be found in Martins et al.'s [26] and Rossi et al.'s [31] work.

### 3.3 Parameter identification procedure

Full-field displacement measurements were presented as a discrete number of data points across the surface of the specimen. To apply the VFM, meshes based on the nodal positions in the deformation field were constructed using the Delaunay triangulation algorithm. Deformation tensors, **F**, were calculated for each mesh element as the average deformation of this element.

The virtual strains under the **QR** framework, $\delta\tilde{\boldsymbol{F}}$, were calculated based on Eq. 19.

As discussed in Sect. 2.2.3, the IVW for **QR** decomposition-based hyperelastic models can be calculated based on the variation of elastic energy caused by virtual displacements, $IVW = \int_{V_0} \delta\bar{W}\left(\mathbf{x}(\mathbf{X}), \mathbf{U}^*\right) \, dV$. Thus, the discrete form of the IVW can be expressed as

$$IVW = \sum_{i=1}^{n_e} \delta\bar{W}\left(\mathbf{x}(\mathbf{X}), \mathbf{U}^*\right) \cdot A_i t_i \tag{23}$$

where $n_e$ represents the total number of mesh elements; $\mathbf{U}^*$ is the virtual displacement, $A_i$ and $t_i$ represent the area and the thickness of a specific element under the reference configuration, $\bar{W}$ is the strain energy density function of the hyperelastic material under **QR** framework, and $\delta\bar{W}(\mathbf{x}(\mathbf{X}), \mathbf{U}^*)$ is the variation of $\bar{W}$, which is denoted as $\delta\bar{W}(\mathbf{U}^*)$ for simplicity in the following derivation. $\delta\bar{W}$ for Mooney–Rivlin model can be expressed as $C_{10}\delta I_1(\tilde{\boldsymbol{F}}) + C_{01}\delta I_2(\tilde{\boldsymbol{F}})$, with $\delta I_1(\tilde{\boldsymbol{F}})$ and $\delta I_2(\tilde{\boldsymbol{F}})$ given in Eq. 21.

In this work, we constructed three virtual fields $(\mathbf{U}_k^{*(a)}, \mathbf{U}_k^{*(b)}, \mathbf{U}_k^{*(c)})$ for each deformation step $k = 1, 2, 3 \ldots N$. According to the principle of virtual work, we have

$$\begin{aligned}
\sum_{i=1}^{n_e} \delta\bar{W}(\mathbf{U}_k^{*(a)}) \cdot A_i t_i &= \delta W_{ext}(\mathbf{U}_k^{*(a)}) \\
\sum_{i=1}^{n_e} \delta\bar{W}(\mathbf{U}_k^{*(b)}) \cdot A_i t_i &= \delta W_{ext}(\mathbf{U}_k^{*(b)}) \\
\sum_{i=1}^{n_e} \delta\bar{W}(\mathbf{U}_k^{*(c)}) \cdot A_i t_i &= \delta W_{ext}(\mathbf{U}_k^{*(c)})
\end{aligned} \tag{24}$$

where $\sum_{i=1}^{n_e} \delta\bar{W}(\mathbf{U}_k^{*(a)}) \cdot A_i t_i$, $\sum_{i=1}^{n_e} \delta\bar{W}(\mathbf{U}_k^{*(b)}) \cdot A_i t_i$, and $\sum_{i=1}^{n_e} \delta\bar{W}(\mathbf{U}_k^{*(c)}) \cdot A_i t_i$ represent the IVW for the three virtual fields, respectively, for deformation step $k$; and $\delta W_{ext}(\mathbf{U}_k^{*(a)})$, $\delta W_{ext}(\mathbf{U}_k^{*(b)})$, and $\delta W_{ext}(\mathbf{U}_k^{*(c)})$ represent the EVW for the three virtual fields, respectively. In the case of **QR**-based Mooney–Rivlin model, we obtained the IVW generated from these three virtual fields for each deformation step $k$ as

$$\begin{aligned}
\delta\bar{W}(\mathbf{U}_k^{*(a)}) &= C_{10} \cdot \delta I_1(\mathbf{U}_k^{*(a)}) + C_{01} \cdot \delta I_2(\mathbf{U}_k^{*(a)}) \\
\delta\bar{W}(\mathbf{U}_k^{*(b)}) &= C_{10} \cdot \delta I_1(\mathbf{U}_k^{*(b)}) + C_{01} \cdot \delta I_2(\mathbf{U}_k^{*(b)}) \\
\delta\bar{W}(\mathbf{U}_k^{*(c)}) &= C_{10} \cdot \delta I_1(\mathbf{U}_k^{*(c)}) + C_{01} \cdot \delta I_2(\mathbf{U}_k^{*(c)})
\end{aligned} \tag{25}$$

Let $a_1(\mathbf{U}_k^{*(a)}) = \sum_{i=1}^{n_e} \delta I_1(\mathbf{U}_k^{*(a)}) \cdot A_i t_i$, $a_2(\mathbf{U}_k^{*(a)}) = \sum_{i=1}^{n_e} \delta I_2(\mathbf{U}_k^{*(a)}) \cdot A_i t_i$, $a_1(\mathbf{U}_k^{*(b)}) = \sum_{i=1}^{n_e} \delta I_1(\mathbf{U}_k^{*(b)}) \cdot A_i t_i$, $a_2(\mathbf{U}_k^{*(b)}) = \sum_{i=1}^{n_e} \delta I_2(\mathbf{U}_k^{*(b)}) \cdot A_i t_i$, $a_1(\mathbf{U}_k^{*(c)}) = \sum_{i=1}^{n_e} \delta I_1(\mathbf{U}_k^{*(c)}) \cdot A_i t_i$, $a_2(\mathbf{U}_k^{*(c)}) = \sum_{i=1}^{n_e} \delta I_2(\mathbf{U}_k^{*(c)}) \cdot A_i t_i$, we could have

$$\begin{aligned}
a_1(\mathbf{U}_k^{*(a)}) \cdot C_{10} + a_2(\mathbf{U}_k^{*(a)}) \cdot C_{01} &= \delta W_{ext}(\mathbf{U}_k^{*(a)}) \\
a_1(\mathbf{U}_k^{*(b)}) \cdot C_{10} + a_2(\mathbf{U}_k^{*(b)}) \cdot C_{01} &= \delta W_{ext}(\mathbf{U}_k^{*(b)})
\end{aligned}$$

$$a_1(\mathbf{U}_k^{*(c)}) \cdot C_{10} + a_2(\mathbf{U}_k^{*(c)}) \cdot C_{01} = \delta W_{ext}(\mathbf{U}_k^{*(c)}) \tag{26}$$

By selecting an appropriate set of virtual fields, $\mathbf{U}_k^*$, constant virtual displacement, $\mathbf{U}_{k_0}^*$, can be formed over the boundaries at which the resultant of the applied load, $\mathbf{F}_{load}$, is known. The EVW, $\delta W_{ext}(\mathbf{U}_k^*)$, is calculated as the multiplication between the measured load at the boundary of the specimen and the constant virtual displacement. Therefore, it can be expressed as follow

$$EVW = \mathbf{U}_{k_0}^* \cdot \int_{\Gamma_0} \mathbf{T} dS = \mathbf{U}_{k_0}^* \cdot \mathbf{F}_{load} \tag{27}$$

Combing the IVW and EVW terms into the matrix form, we obtained

$$\begin{bmatrix} a_1(\mathbf{U}_k^{*(a)}) & a_2(\mathbf{U}_k^{*(a)}) \\ a_1(\mathbf{U}_k^{*(b)}) & a_2(\mathbf{U}_k^{*(b)}) \\ a_1(\mathbf{U}_k^{*(c)}) & a_2(\mathbf{U}_k^{*(c)}) \end{bmatrix} \begin{bmatrix} C_{10} \\ C_{01} \end{bmatrix} = \begin{bmatrix} \delta W_{ext}(\mathbf{U}_k^{*(a)}) \\ \delta W_{ext}(\mathbf{U}_k^{*(b)}) \\ \delta W_{ext}(\mathbf{U}_k^{*(c)}) \end{bmatrix} \tag{28}$$

for each deformation step. Assembling the equations of all the deformation steps, we could have the following matrix

$$\begin{bmatrix} a_1(\mathbf{U}_1^{*(a)}) & a_2(\mathbf{U}_1^{*(a)}) \\ a_1(\mathbf{U}_1^{*(b)}) & a_2(\mathbf{U}_1^{*(b)}) \\ a_1(\mathbf{U}_1^{*(c)}) & a_2(\mathbf{U}_1^{*(c)}) \\ \cdots & \\ a_1(\mathbf{U}_N^{*(a)}) & a_2(\mathbf{U}_N^{*(a)}) \\ a_1(\mathbf{U}_N^{*(b)}) & a_2(\mathbf{U}_N^{*(b)}) \\ a_1(\mathbf{U}_N^{*(c)}) & a_2(\mathbf{U}_N^{*(c)}) \end{bmatrix} \begin{bmatrix} C_{10} \\ C_{01} \end{bmatrix} = \begin{bmatrix} \delta W_{ext}(\mathbf{U}_1^{*(a)}) \\ \delta W_{ext}(\mathbf{U}_1^{*(b)}) \\ \delta W_{ext}(\mathbf{U}_1^{*(c)}) \\ \cdots \\ \delta W_{ext}(\mathbf{U}_N^{*(a)}) \\ \delta W_{ext}(\mathbf{U}_N^{*(b)}) \\ \delta W_{ext}(\mathbf{U}_N^{*(c)}) \end{bmatrix} \tag{29}$$

Let the $3N \times 2$ matrix on the left-hand side of the above equation be $\mathbf{A}$, $\boldsymbol{\beta} = [C_{10}, C_{01}]^T$, and the $3N$-dimensional vector on the right-hand side be $\mathbf{y}$, Eq. 29 can be expressed as

$$\mathbf{A}\boldsymbol{\beta} = \mathbf{y} \tag{30}$$

Note that the number of equations is more than that of the unknowns (only two unknowns, $C_{10}$ and $C_{01}$). Therefore, we can use the least square method to solve the material parameters $C_{10}$ and $C_{01}$ as

$$\boldsymbol{\beta} = (\mathbf{A}^T\mathbf{A})^{-1}\mathbf{A}^T\mathbf{y} \tag{31}$$

The parameter identification procedure for hyperelastic models under polar decomposition is similar, which can be found in "Appendix D".

## 4 Results

### 4.1 Strain field measurement and parameter identification

A typical view of the $E_{11}$, $E_{22}$, and $E_{12}$ distributions (components from the Green strain tensor) over the selected ROI is shown in Fig. 3. The applied global strains along both axes were 1.5. The symmetry of these distributions provides evidence of the good alignment achieved in the testing platform.

Figures 4 and 5 depict the deformation distributions and distortion distributions across the selected ROI, respectively. Under the equi-biaxial tension states, the $F_{11}$ distribution is symmetric to the $F_{22}$ distribution; the $F_{12}$ distribution is symmetric to the $F_{21}$ distribution, which further demonstrates the good alignment achieved in the experimental setup. However, the $\widetilde{F}_{11}$ distribution is unsymmetrical to the $\widetilde{F}_{22}$ distribution under the **QR** decomposition framework.

$\widetilde{F}_{11}$ is always larger than $F_{11}$ at each data point due to the existence of the term of $F_{21}$. However, in the arm area and the center gage zone where $F_{21}$ is close to zero, $\widetilde{F}_{11}$, $\widetilde{F}_{12}$, and $\widetilde{F}_{22}$ are nearly equal to $F_{11}$, $F_{12}$, and $F_{22}$, respectively.

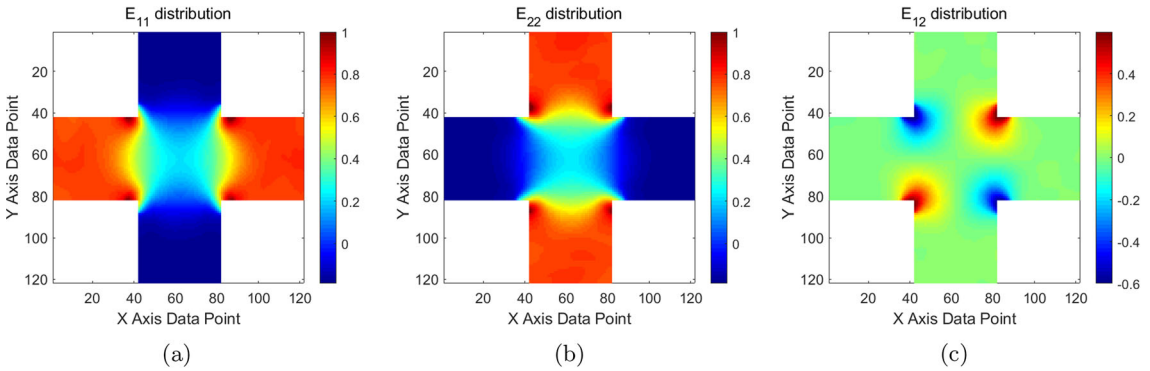


**Fig. 3** Green strain distributions over the selected ROI of Specimen C under an equi-biaxial test. **a** $E_{11}$ distribution; **b** $E_{22}$ distribution; **c** $E_{12}$ distribution. The symmetry of the strain distributions denotes that good alignment was achieved in the biaxial system

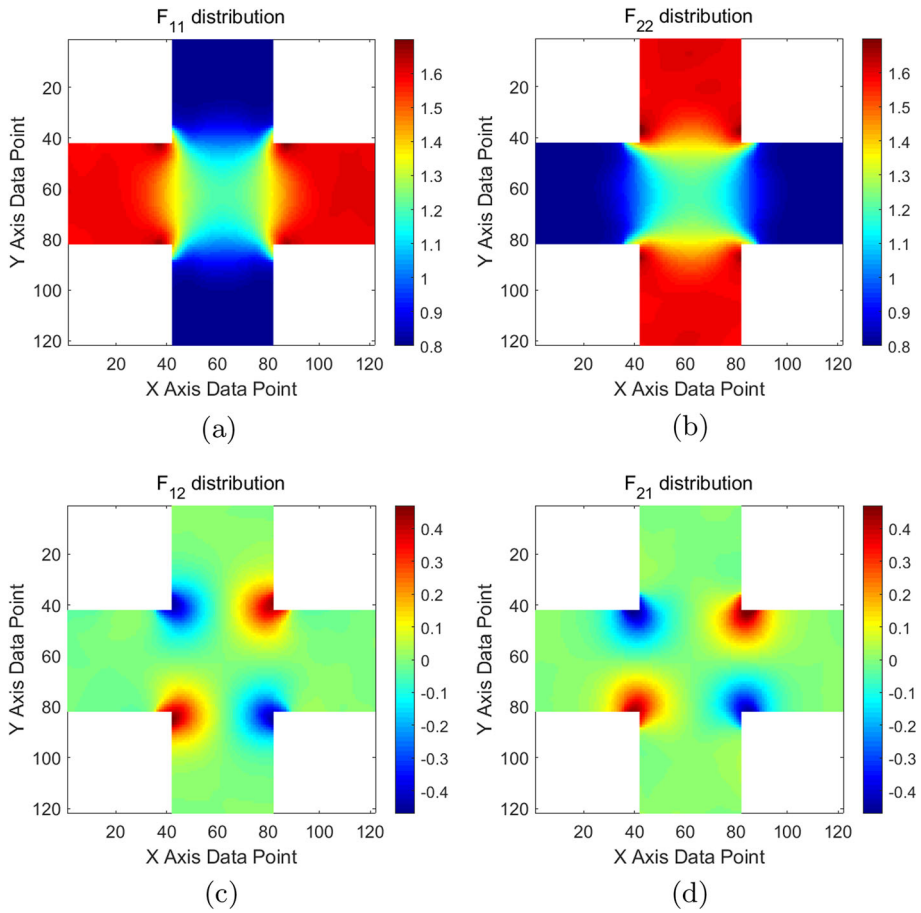


**Fig. 4** Deformation gradient **F** distributions (polar decomposition) over the selected ROI of Specimen C under an equi-biaxial test. **a** $F_{11}$ distribution; **b** $F_{22}$ distribution; **c** $F_{12}$ distribution; **d** $F_{21}$ distribution. The symmetry of the deformation distributions denote that good alignment was achieved in the biaxial system

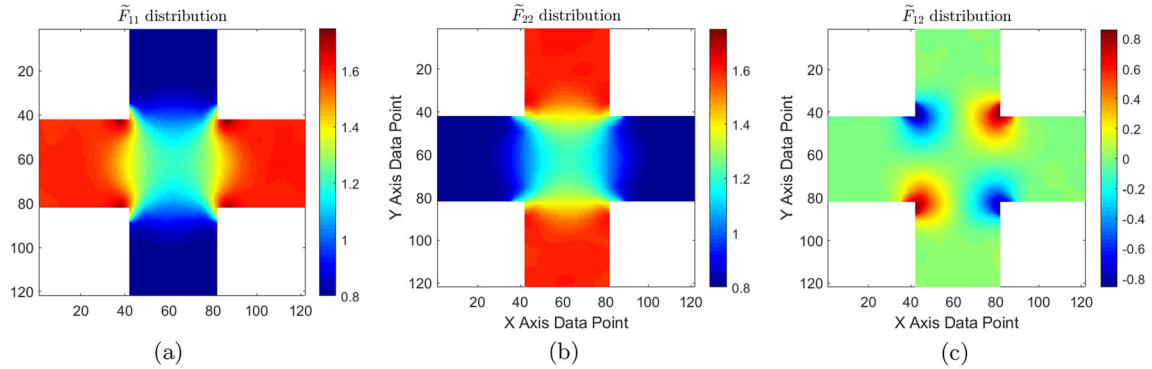


**Fig. 5** Distortion tensor $\widetilde{\boldsymbol{F}}$ distributions (**QR** decomposition) over the selected ROI of Specimen C under an equi-biaxial test. **a** $\widetilde{F}_{11}$ distribution; **b** $\widetilde{F}_{22}$ distribution; **c** $\widetilde{F}_{12}$ distribution

Parameters of hyperelastic models were obtained from full-field deformation data observed in biaxial tensile tests for three specimens. Since each hyperelastic model and its corresponding **QR** form are mathematically equivalent, the extracted material parameters for each pair of models should be equal to each other. The parameters of the conventional and QR decomposition-based neo-Hookean models are the same ($C_{10} = 0.2117, 0.2125, 0.2123$ MPa for three specimens); the parameters of the conventional and QR decomposition-based Mooney–Rivlin models are also the same ($C_{10} = 0.1741, 0.1761, 0.1763$ MPa and $C_{01} = 0.0440, 0.0423, 0.0416$ MPa for three specimens), which indicate that the proposed VFM works well for QR decomposition-based hyperelastic models.

## 4.2 Stress reconstruction

Cauchy stress under both polar decomposition and **QR** decomposition frameworks were reconstructed across the selected ROI based on the deformation measurement and extracted parameters. Cauchy stress under the polar decomposition framework is expressed as

$$\sigma = \frac{\partial W}{\partial \mathbf{F}}\mathbf{F}^T - p\mathbf{I} \tag{32}$$

The rotated Cauchy stress under **QR** decomposition is expressed as

$$\widetilde{\sigma} = \frac{\partial \bar{W}}{\partial \widetilde{\mathbf{F}}}\widetilde{\mathbf{F}}^T - \widetilde{p}\mathbf{I} \tag{33}$$

where $\widetilde{p}$ is the hydrostatic pressure.

$$\begin{aligned}
\widetilde{\sigma}_{11} &= \frac{\partial \bar{W}}{\partial \widetilde{F}_{11}}\widetilde{F}_{11} + \frac{\partial \bar{W}}{\partial \widetilde{F}_{12}}\widetilde{F}_{12} - \widetilde{p} \\
\widetilde{\sigma}_{22} &= \frac{\partial \bar{W}}{\partial \widetilde{F}_{22}}\widetilde{F}_{22} - \widetilde{p} \\
\widetilde{\sigma}_{33} &= \frac{\partial \bar{W}}{\partial \widetilde{F}_{33}}\widetilde{F}_{33} - \widetilde{p} \\
\widetilde{\sigma}_{12} &= \frac{\partial \bar{W}}{\partial \widetilde{F}_{12}}\widetilde{F}_{22}
\end{aligned} \tag{34}$$

Herein, $\widetilde{p} = 2C_{10}\widetilde{F}_{33}^2 + 2C_{01}\widetilde{F}_{33}^2(\widetilde{F}_{11}^2 + \widetilde{F}_{22}^2 + \widetilde{F}_{12}^2)$ with $\widetilde{F}_{33} = \frac{1}{\widetilde{F}_{11}\widetilde{F}_{22}}$.

Cauchy stress distributions for the two models under polar decomposition and **QR** decomposition are presented in Figs. 6 and 7, respectively. Under the equi-biaxial tension, the $\sigma_{11}$ distribution is symmetric to the $\sigma_{22}$ distribution; however, the $\widetilde{\sigma}_{11}$ distribution is unsymmetrical to the $\widetilde{\sigma}_{22}$ distribution.

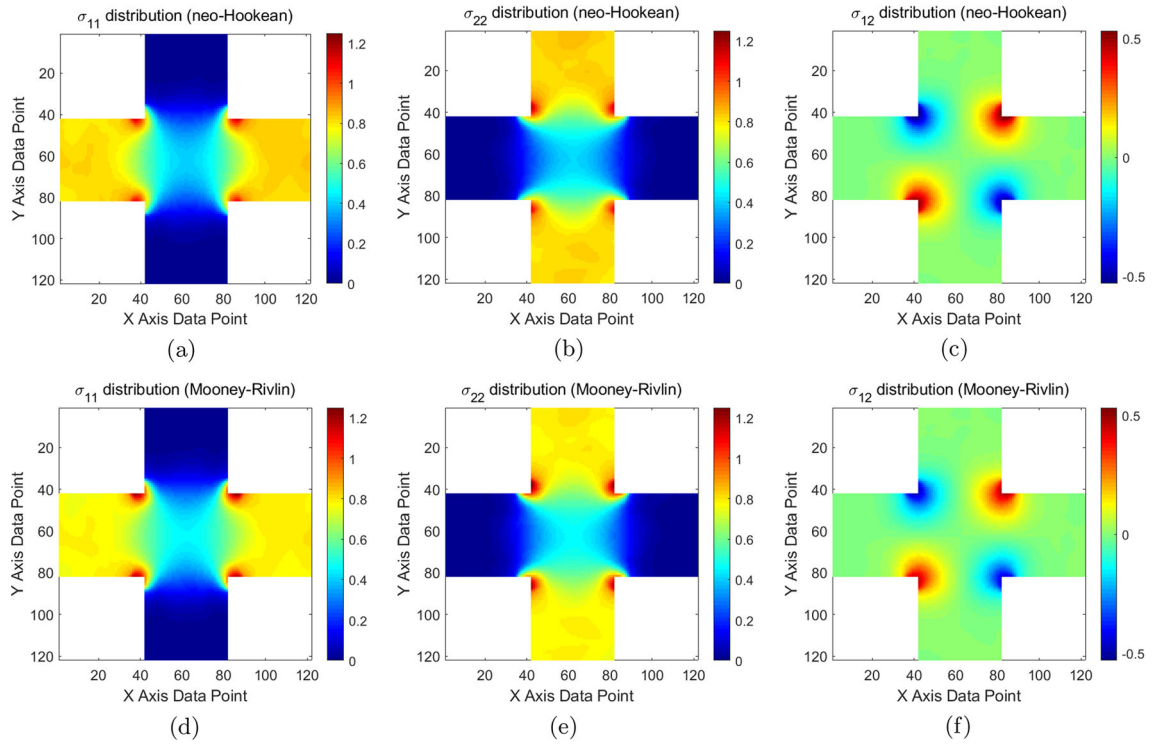


**Fig. 6** Cauchy stress distributions (under ploar decomposition) over the selected ROI of Specimen C under an equi-biaxial test. **a** $\sigma_{11}$ distribution; **b** $\sigma_{22}$ distribution; **c** $\sigma_{12}$ distribution. Stress were reconstructed based on full-field deformation data and extracted material parameters

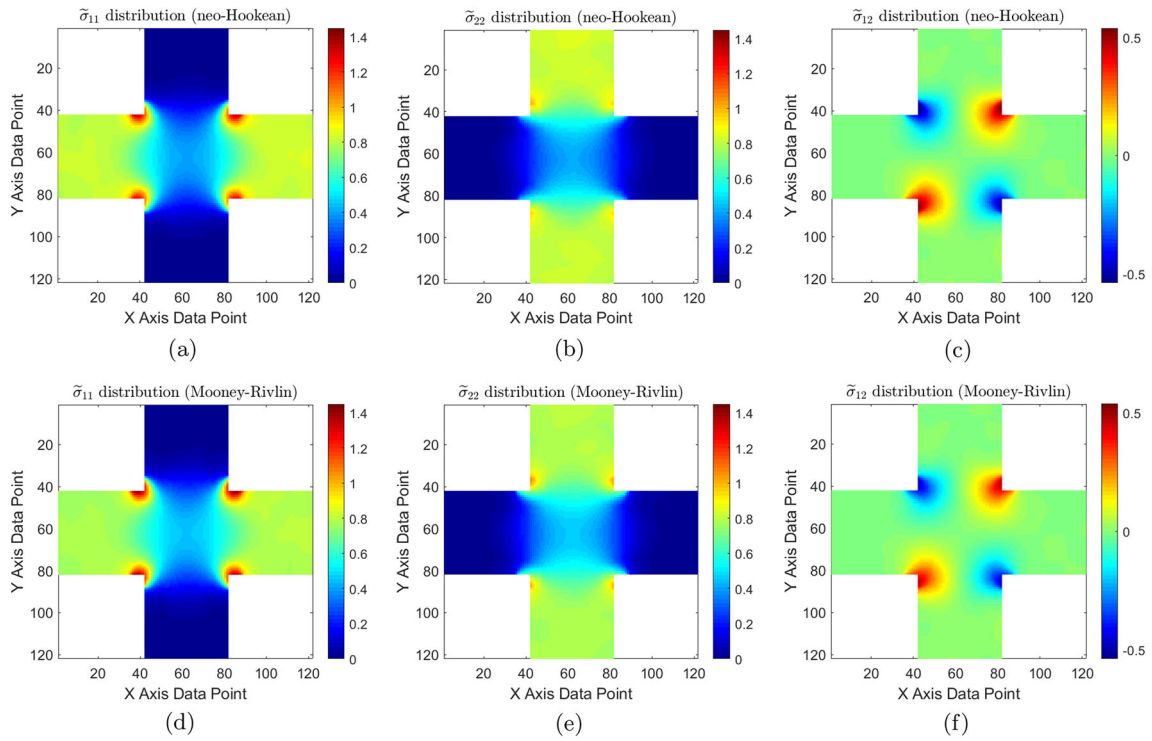


**Fig. 7** Cauchy stress distributions (under **QR** framework) for Specimen C under an equi-biaxial test. **a** $\widetilde{\sigma}_{11}$ distribution; **b** $\widetilde{\sigma}_{22}$ distribution; **c** $\widetilde{\sigma}_{12}$ distribution

## 5 Summary

**QR** decomposition-based hyperelastic models proposed in recent years have unique advantages over conventional one, as the components of the distortion tensor have clear physical meanings. However, systematic works on parameter identification of these hyperelastic models are lacking. In this work, we propose the VEE-VFM which considers the IVW of the VFM as the variation of elastic energy caused by virtual displacements. This fundamental explanation of the IVW leads to two main advantages of VEE-VFM over the conventional one. (a) Conventional VFM requires Cauchy stress, the first, or second Piola–Kirchhoff stress, and their conjugate virtual strains to calculate the IVW, while there are no specific requirements on the types of stresses in VEE-VFM. For conventional invariant-based hyperelastic models, this advantage may not be obvious, but for the **QR** decomposition and principal stretch-based hyperelastic models, which cannot result in Cauchy stress and Piola–Kirchhoff stress directly, the VEE-VFM can avoid stresses transformations and thus is more concise. (b) VEE-VFM can automatically guarantee the conjugate relation between the stresses and virtual strains used to calculate the IVW. Therefore, the VEE-VFM is easier to be implemented than conventional VFM, particularly for **QR** decomposition and principal stretch-based hyperelastic models. Finally, we extract the parameters of the derived Mooney–Rivlin model under the **QR** framework to validate the proposed VEE-VFM. As this method can be easily extended to parameter identification of any other **QR** decomposition-based hyperelastic models, in the future, we will extend it to anisotropic models.

**Acknowledgements** This work was supported by Anhui Provincial Natural Science Foundation under Grant No. 2108085ME163; the Fundamental Research Funds for the Central Universities under Grant Nos. JZ2020HGQA0183 and JZ2021HGTA0161; Hefei 2021 Innovation and Entrepreneurship Support Plan for Returned Overseas Students; and the Innovation Seed Project Funding and Startup Funding (No. ST2100023) provided by Guangdong Technion - Israel Institute of Technology.

## Appendix A Derivation of IVW based on Promma and Grediac's approach

Assuming that the material was incompressible and a plane-stress condition, we can have the deformation gradient tensor expressed as

$$\mathbf{F} = \begin{bmatrix} F_{11} & F_{12} & 0 \\ F_{21} & F_{22} & 0 \\ 0 & 0 & \frac{1}{D} \end{bmatrix} \tag{A.1}$$

with $D = F_{11}F_{22} - F_{12}F_{21}$. Therefore, we have

$$\mathbf{F}^{-T} = \frac{1}{D}\begin{bmatrix} F_{22} & -F_{21} & 0 \\ -F_{12} & F_{11} & 0 \\ 0 & 0 & D^2 \end{bmatrix} \tag{A.2}$$

and

$$\mathbf{C} = \mathbf{F}^T\mathbf{F} = \begin{bmatrix} F_{11}^2 + F_{21}^2 & F_{11}F_{12} + F_{21}F_{22} & 0 \\ F_{11}F_{12} + F_{21}F_{22} & F_{12}^2 + F_{22}^2 & 0 \\ 0 & 0 & \frac{1}{D^2} \end{bmatrix} \tag{A.3}$$

According to Eq. 32, Cauchy stress components of Mooney–Rivlin model are

$$\begin{aligned} \sigma_{11} &= 2C_{10}\left(F_{11}^2 + F_{12}^2 - \frac{1}{D^2}\right) + 2C_{01}\left(D^2 - \frac{F_{21}^2}{D^2} - \frac{F_{22}^2}{D^2}\right) \\ \sigma_{22} &= 2C_{10}\left(F_{21}^2 + F_{22}^2 - \frac{1}{D^2}\right) + 2C_{01}\left(D^2 - \frac{F_{11}^2}{D^2} - \frac{F_{12}^2}{D^2}\right) \\ \sigma_{12} &= 2C_{10}(F_{12}F_{22} + F_{11}F_{21}) + 2C_{01}\frac{1}{D^2}(F_{12}F_{22} + F_{11}F_{21}) \end{aligned} \tag{A.4}$$

The first Piola–Kirchhoff stress $\mathbf{P}$ is derived from Cauchy stress tensor $\boldsymbol{\sigma}$ using the following expression:

$$\mathbf{P} = J\sigma\mathbf{F}^{-T} \tag{A.5}$$

with $J = 1$ for incompressible materials. We obtain the first Piola–Kirchhoff stress whose components are expressed as below

$$
\begin{aligned}
P_{11} &= 2C_{10}\left(-\frac{F_{22}}{D^3} + F_{11}\right) + 2C_{01}\left(-\frac{F_{22}}{D^3}(F_{11}^2 + F_{21}^2 + F_{12}^2 + F_{22}^2) + F_{22}D + \frac{F_{11}}{D^2}\right) \\
P_{12} &= 2C_{10}\left(\frac{F_{21}}{D^3} + F_{12}\right) + 2C_{01}\left(\frac{F_{21}}{D^3}(F_{11}^2 + F_{21}^2 + F_{12}^2 + F_{22}^2) - F_{21}D + \frac{F_{12}}{D^2}\right) \\
P_{21} &= 2C_{10}\left(\frac{F_{12}}{D^3} + F_{21}\right) + 2C_{01}\left(\frac{F_{12}}{D^3}(F_{11}^2 + F_{21}^2 + F_{12}^2 + F_{22}^2) - F_{12}D + \frac{F_{21}}{D^2}\right) \\
P_{22} &= 2C_{10}\left(-\frac{F_{11}}{D^3} + F_{22}\right) + 2C_{01}\left(-\frac{F_{11}}{D^3}(F_{11}^2 + F_{21}^2 + F_{12}^2 + F_{22}^2) + F_{11}D + \frac{F_{22}}{D^2}\right)
\end{aligned}
\tag{A.6}
$$

The derivative of virtual displacement[2] is written as follows:

$$
\frac{\partial \mathbf{U}^*}{\partial \mathbf{X}} = \frac{\partial \boldsymbol{\delta U}}{\partial \mathbf{X}} = \delta \frac{\partial \mathbf{U}}{\partial \mathbf{X}} \tag{A.7}
$$

The virtual displacement field $\delta\mathbf{u}$ is independent of the actual displacement field $\mathbf{u}$ and can be expressed in terms of spatial coordinates or material coordinates. Therefore, we have $\delta\mathbf{U} = \delta\mathbf{u}$

$$
\delta \frac{\partial \mathbf{U}}{\partial \mathbf{X}} = \delta \frac{\partial \mathbf{u}}{\partial \mathbf{X}} = \delta(\mathbf{F} - \mathbf{I}) = \delta\mathbf{F} \tag{A.8}
$$

Therefore, the IVW for a single mesh element within the body of the specimen is written as follows:

$$
\mathbf{P} : \frac{\partial \mathbf{U}^*}{\partial \mathbf{X}} = \mathbf{P} : \delta\mathbf{F} = P_{11}\delta F_{11} + P_{12}\delta F_{12} + P_{21}\delta F_{21} + P_{22}\delta F_{22} \tag{A.9}
$$

After plugging the components of the first Piola–Kirchhoff stress (Eq. A.6) into the above equation, we can find the formulation of IVW for hyperelastic materials based on the conventional VFM proposed by Promma and Grediac [20] is equivalent to the formulation of IVW in VEE-VFM (Eq. 13).

## Appendix B Detailed expression of $\delta\widetilde{F}$

$$
\delta\widetilde{F}_{11} = \frac{\partial \widetilde{F}_{11}}{\partial F_{11}}\delta F_{11} + \frac{\partial \widetilde{F}_{11}}{\partial F_{21}}\delta F_{21} \tag{B.1}
$$

with

$$
\frac{\partial \widetilde{F}_{11}}{\partial F_{11}} = \frac{F_{11}}{\sqrt{F_{11}^2 + F_{21}^2}}, \quad \frac{\partial \widetilde{F}_{11}}{\partial F_{21}} = \frac{F_{21}}{\sqrt{F_{11}^2 + F_{21}^2}} \tag{B.2}
$$

$$
\delta\widetilde{F}_{12} = \frac{\partial \widetilde{F}_{12}}{\partial F_{11}}\delta F_{11} + \frac{\partial \widetilde{F}_{12}}{\partial F_{12}}\delta F_{12} + \frac{\partial \widetilde{F}_{12}}{\partial F_{21}}\delta F_{21} + \frac{\partial \widetilde{F}_{12}}{\partial F_{22}}\delta F_{22} \tag{B.3}
$$

with

$$
\begin{aligned}
\frac{\partial \widetilde{F}_{12}}{\partial F_{11}} &= \frac{F_{21}(F_{12}F_{21} - F_{11}F_{22})}{(F_{11}^2 + F_{21}^2)\sqrt{F_{11}^2 + F_{21}^2}} \\
\frac{\partial \widetilde{F}_{12}}{\partial F_{21}} &= \frac{F_{11}(F_{11}F_{22} - F_{12}F_{21})}{(F_{11}^2 + F_{21}^2)\sqrt{F_{11}^2 + F_{21}^2}} \\
\frac{\partial \widetilde{F}_{12}}{\partial F_{12}} &= \frac{F_{11}}{\sqrt{F_{11}^2 + F_{21}^2}}
\end{aligned}
$$

[2] Promma and Grediac used $\mathbf{U}^*$ to denote the virtual displacement, we used $\delta\mathbf{U}$ in this section.

$$\frac{\partial \widetilde{F}_{12}}{\partial F_{22}} = \frac{F_{21}}{\sqrt{F_{11}^2 + F_{21}^2}} \tag{B.4}$$

$$\delta \widetilde{F}_{22} = \frac{\partial \widetilde{F}_{22}}{\partial F_{11}}\delta F_{11} + \frac{\partial \widetilde{F}_{22}}{\partial F_{12}}\delta F_{12} + \frac{\partial \widetilde{F}_{22}}{\partial F_{21}}\delta F_{21} + \frac{\partial \widetilde{F}_{22}}{\partial F_{22}}\delta F_{22} \tag{B.5}$$

with

$$\begin{aligned}
\frac{\partial \widetilde{F}_{22}}{\partial F_{11}} &= \frac{F_{22}(F_{11}F_{22} - F_{12}F_{21})(F_{11}^2 + F_{21}^2) - F_{11}(F_{11}F_{22} - F_{12}F_{21})^2}{(F_{11}^2 + F_{21}^2)^2\sqrt{(F_{11}F_{22} - F_{12}F_{21})^2}}\sqrt{F_{11}^2 + F_{21}^2} \\
\frac{\partial \widetilde{F}_{22}}{\partial F_{21}} &= \frac{F_{12}(F_{12}F_{21} - F_{11}F_{22})(F_{11}^2 + F_{21}^2) - F_{21}(F_{11}F_{22} - F_{12}F_{21})^2}{(F_{11}^2 + F_{21}^2)^2\sqrt{(F_{11}F_{22} - F_{12}F_{21})^2}}\sqrt{F_{11}^2 + F_{21}^2} \\
\frac{\partial \widetilde{F}_{22}}{\partial F_{12}} &= \frac{F_{21}(F_{12}F_{21} - F_{11}F_{22})}{\sqrt{F_{11}^2 + F_{21}^2}\sqrt{(F_{11}F_{22} - F_{12}F_{21})^2}} \\
\frac{\partial \widetilde{F}_{22}}{\partial F_{22}} &= \frac{F_{11}(F_{11}F_{22} - F_{12}F_{21})}{\sqrt{F_{11}^2 + F_{21}^2}\sqrt{(F_{11}F_{22} - F_{12}F_{21})^2}}
\end{aligned} \tag{B.6}$$

$$\delta \widetilde{F}_{33} = \frac{\partial \widetilde{F}_{22}}{\partial F_{11}}\delta F_{11} + \frac{\partial \widetilde{F}_{33}}{\partial F_{12}}\delta F_{12} + \frac{\partial \widetilde{F}_{33}}{\partial F_{21}}\delta F_{21} + \frac{\partial \widetilde{F}_{33}}{\partial F_{22}}\delta F_{22} \tag{B.7}$$

with

$$\begin{aligned}
\frac{\partial \widetilde{F}_{33}}{\partial F_{11}} &= -\frac{F_{33}\sqrt{(F_{11}F_{22} - F_{12}F_{21})^2}}{(F_{11}F_{22} - F_{12}F_{21})^3} \\
\frac{\partial \widetilde{F}_{33}}{\partial F_{21}} &= -\frac{F_{12}\sqrt{(F_{11}F_{22} - F_{12}F_{21})^2}}{(F_{11}F_{22} - F_{12}F_{21})^3} \\
\frac{\partial \widetilde{F}_{33}}{\partial F_{12}} &= -\frac{F_{21}\sqrt{(F_{11}F_{22} - F_{12}F_{21})^2}}{(F_{11}F_{22} - F_{12}F_{21})^3} \\
\frac{\partial \widetilde{F}_{33}}{\partial F_{22}} &= -\frac{F_{11}\sqrt{(F_{11}F_{22} - F_{12}F_{21})^2}}{(F_{11}F_{22} - F_{12}F_{21})^3}
\end{aligned} \tag{B.8}$$

## Appendix C Incompressibility justification

Uniaxial tensile tests were performed on rectangular silicone elastomer. Three specimens were tested up to 60% strain under a strain rate of 1%/s. Ncorr, a Matlab-based digital image correlation software, was used

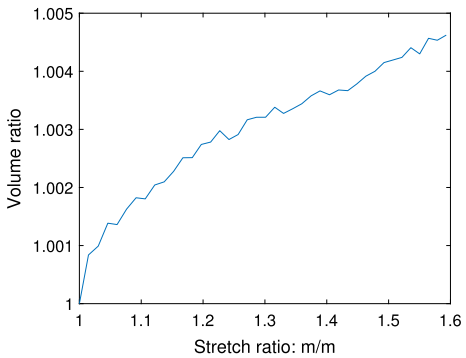


**Fig. 8** The change of the ratio between the current and initial volume of the specimens with the stretch ratio (averaged from three specimens) under uniaxial tension

for strain measurement across the surface of the specimens. A rectangular ROI which was far away from the clamps was selected for data analysis. The strain within this region was uniformly distributed. Details about the testing protocol can be found in this paper [28]. The stretch ratio along the stretching direction ($\lambda_x$) and stretch ratio across the stretching direction ($\lambda_y$) were extracted and averaged over the selected ROI. Since specimens were under uniaxial tension, we assumed that $\lambda_y = \lambda_z$. Therefore, the ratio of the current volume over the initial volume was calculated as $\lambda_x * {\lambda_y}^2$. Figure 8 shows that the ratio between the current and initial volumes slightly increases with the stretch ratio. The maximum change of the volume occurred in the last deformation step, which was about 0.46%. This small difference can be considered negligible. Therefore, the material can be assumed to be incompressible.

## Appendix D Parameter identification with VEE-VFM for Mooney–Rivlin model under polar decomposition

After extracting the full-field displacement data and forming triangular mesh elements based on nodal positions, the deformation gradient and virtual strain can be calculated respectively. The integral of the IVW for a hyperelastic model under polar decomposition in Eq. 12 can be approximated by a discrete sum as follows

$$IVW = \sum_{i=1}^{n_e} \delta W\left(\mathbf{x}(\mathbf{X}), \mathbf{U}^*\right) \cdot A_i t_i \tag{D.1}$$

where $n_e$ represents the total number of mesh elements; and $A_i$ and $t_i$ represent the area and the thickness of a specific element under the reference configuration, which do not depend on time; $W$ is the strain energy density function of the hyperelastic material. Note that $\delta W$ for Mooney–Rivlin model under the polar decomposition is expressed as $C_{10}\delta I_1 + C_{01}\delta I_2$. $\delta I_1$ and $\delta I_2$ can be calculated based on Eq. 15.
For each deformation step $k$, we can construct one virtual field $\mathbf{U}_k^*$. According to the principle of virtual work, we have

$$\sum_{i=1}^{n_e} \delta W(\mathbf{U}_k^*) \cdot A_i t_i = \delta W_{ext}(\mathbf{U}_k^*) \tag{D.2}$$

where $\sum_{i=1}^{n_e} \delta W(\mathbf{U}_k^*) \cdot A_i t_i$ represents the sum of the IVW of all the mesh elements, and $\delta W_{ext}(\mathbf{U}_k^*)$ represents the EVW. In the case of Mooney–Rivlin model, $\delta W(\mathbf{U}_k^*)$ is expressed as

$$\delta W(\mathbf{U}_k^*) = C_{10} \cdot \delta I_1(\mathbf{U}_k^*) + C_{01} \cdot \delta I_2(\mathbf{U}_k^*) \tag{D.3}$$

Therefore, we can have

$$\sum_{i=1}^{n_e} (C_{10} \cdot \delta I_1(\mathbf{U}_k^*) + C_{01} \cdot \delta I_2(\mathbf{U}_k^*)) \cdot A_i t_i = \delta W_{ext}(\mathbf{U}^*) \tag{D.4}$$

Note that we constructed three virtual fields in this paper. The rest of the procedure to identify material parameters is the same as that described in Sect. 3.3.

## References


1. McLellan, A.: Invariant functions and homogeneous bases of irreducible representations of the crystal point groups, with applications to thermodynamic properties of crystals under strain. J. Phys. C Solid State Phys. **7**(18), 3326 (1974)
2. McLellan, A.: Finite strain coordinates and the stability of solid phases. J. Phys. C Solid State Phys. **9**(22), 4083 (1976)
3. Srinivasa, A.: On the use of the upper triangular (or QR) decomposition for developing constitutive equations for green-elastic materials. Int. J. Eng. Sci. **60**, 1–12 (2012)
4. Ghosh, P., Srinivasa, A.: Development of a finite strain two-network model for shape memory polymers using QR decomposition. Int. J. Eng. Sci. **81**, 177–191 (2014)
5. Freed, A.D., Srinivasa, A.: Logarithmic strain and its material derivative for a QR decomposition of the deformation gradient. Acta Mech. **226**(8), 2645–2670 (2015)
6. Kazerooni, N.A., Srinivasa, A., Freed, A.: Orthotropic-equivalent strain measures and their application to the elastic response of porcine skin. Mech. Res. Commun. **101**, 103404 (2019)
7. Freed, A.D., le Graverend, J.-B., Rajagopal, K.: A decomposition of laplace stretch with applications in inelasticity. Acta Mech. **230**(9), 3423–3429 (2019)

8. Freed, A.D., Zamani, S., Szabó, L., Clayton, J.D.: Laplace stretch: Eulerian and Lagrangian formulations. Z. Angew. Math. Phys. **71**, 157 (2020)
9. Gao, X.-L., Li, Y.: The upper triangular decomposition of the deformation gradient: possible decompositions of the distortion tensor. Acta Mech. **229**(5), 1927–1948 (2018)
10. Li, Y., Gao, X.-L.: Constitutive equations for hyperelastic materials based on the upper triangular decomposition of the deformation gradient. Math. Mech. Solids **24**(6), 1785–1799 (2019)
11. Salamatova, V.Y., Vassilevski, Y.V., Wang, L.: Finite element models of hyperelastic materials based on a new strain measure. Differ. Equ. **54**(7), 971–978 (2018)
12. Annin, B.D., Bagrov, K.V.: Numerical simulation of the hyperelastic material using new strain measure. Acta Mech. **232**(5), 1809–1813 (2021)
13. Freed, A.D., Zamani, S.: On the use of convected coordinate systems in the mechanics of continuous media derived from a QR factorization of F. Int. J. Eng. Sci. **127**, 145–161 (2018)
14. Zamani, S., Paul, S., Kotiya, A.A., Criscione, J.C., Freed, A.D.: Application of QR framework in modeling the constitutive behavior of porcine coronary sinus tissue. Mech. Soft Mater. **3**, 7 (2021)
15. Clayton, J., Freed, A.: A constitutive framework for finite viscoelasticity and damage based on the gram-schmidt decomposition. Acta Mech. **231**(8), 3319–3362 (2020)
16. Clayton, J.D., Freed, A.: A constitutive model for lung mechanics and injury applicable to static, dynamic, and shock loading. Mech. Soft Mater. **2**, 3 (2020)
17. Rivlin, R.S., Saunders, D.: Large elastic deformations of isotropic materials vii experiments on the deformation of rubber. Philos. Trans. R. Soc. Lond. Ser. A Math. Phys. Sci. **243**(865), 251–288 (1951)
18. Ogden, R.W., Saccomandi, G., Sgura, I.: Fitting hyperelastic models to experimental data. Comput. Mech. **34**(6), 484–502 (2004)
19. Kazerooni, N.A., Wang, Z., Srinivasa, A., Criscione, J.: Inferring material parameters from imprecise experiments on soft materials by virtual fields method. Ann. Solid Struct. Mech. **12**, 59–72 (2020)
20. Promma, N., Raka, B., Grediac, M., Toussaint, E., Le Cam, J.-B., Balandraud, X., Hild, F.: Application of the virtual fields method to mechanical characterization of elastomeric materials. Int. J. Solids Struct. **46**(3–4), 698–715 (2009)
21. Tayeb, A., Le Cam, J.B., Grédiac, M., Toussaint, E., Robin, E., Balandraud, X., Canévet, F.: Identifying hyperelastic constitutive parameters with sensitivity-based virtual fields. Strain **57**(6), 12397 (2021)
22. Jiang, M., Wang, Z., Freed, A.D., Moreno, M.R., Erel, V., Dubrowski, A.: Extracting material parameters of silicone elastomers under biaxial tensile tests using virtual fields method and investigating the effect of missing deformation data close to specimen edges on parameter identification. Mech. Adv. Mater. Struct. **29**(27), 6421–6435 (2022)
23. Criscione, J.C., Douglas, A.S., Hunter, W.C.: Physically based strain invariant set for materials exhibiting transversely isotropic behavior. J. Mech. Phys. Solids **49**(4), 871–897 (2001)
24. Criscione, J., Hunter, W.: Kinematics and elasticity framework for materials with two fiber families. Continuum Mech. Thermodyn. **15**, 613–628 (2003)
25. Pierron, F., Grédiac, M.: The Virtual Fields Method: Extracting Constitutive Mechanical Parameters from Full-field Deformation Measurements. Springer, Berlin (2012)
26. Martins, J., Andrade-Campos, A., Thuillier, S.: Calibration of anisotropic plasticity models using a biaxial test and the virtual fields method. Int. J. Solids Struct. **172**, 21–37 (2019)
27. Marek, A., Davis, F.M., Rossi, M., Pierron, F.: Extension of the sensitivity-based virtual fields to large deformation anisotropic plasticity. Int. J. Mater. Form. **12**(3), 457–476 (2019)
28. Jiang, M., Sridhar, R.L., Robbins, A.B., Freed, A.D., Moreno, M.R.: A versatile biaxial testing platform for soft tissues. J. Mech. Behav. Biomed. Mater. **114**, 104144 (2021)
29. Blaber, J., Adair, B., Antoniou, A.: Ncorr: open-source 2d digital image correlation matlab software. Exp. Mech. **55**(6), 1105–1122 (2015)
30. Jiang, M., Dai, J., Dong, G., Wang, Z.: A comparative study of invariant-based hyperelastic models for silicone elastomers under biaxial deformation with the virtual fields method. J. Mech. Behav. Biomed. Mater. **136**, 105522 (2022)
31. Rossi, M., Pierron, F., Štamborská, M.: Application of the virtual fields method to large strain anisotropic plasticity. Int. J. Solids Struct. **97**, 322–335 (2016)